HHS Public Access

Author manuscript

ACS Appl Mater Interfaces. Author manuscript; available in PMC 2018 August 20.

Published in final edited form as:

ACS Appl Mater Interfaces. 2018 July 05; 10(26): 21920–21926. doi:10.1021/acsami.8b06633.

Smaller CpG-conjugated Gold Nanoconstructs Achieve Higher Targeting Specificity of Immune Activation

Jun Yue[1], **Roger M. Pallares**[1], **Lisa E. Cole**[1], **Emma E. Coughlin**[1], **Chad A. Mirkin**[1,2,3], **Andrew Lee**[4], and **Teri W. Odom**[1,2,3,*]

[1]Department of Chemistry, Northwestern University, Evanston, Illinois 60208, United States

[2]Department of Materials Science and Engineering, Northwestern University, Evanston, Illinois 60208, United States

[3]International Institute for Nanotechnology, Northwestern University, Evanston, Illinois 60208, United States

[4]Department of Chemical and Biological Engineering, Northwestern University, Evanston, Illinois 60208, United Statesm

Abstract

This paper describes a side-by-side comparison of the *in vitro* immunostimulatory activity of CpG-conjugated gold nanoparticles. Three different gold nanoparticle cores (13-nm spheres, 50-nm spheres, and 40-nm stars) with the same CpG surface density were investigated for toll-like receptor 9 activation. For this parameter set, 13-nm spheres displayed significantly higher specificity for targeting immune receptors and larger nanoparticles (50-nm spheres and 40-nm stars) showed higher cellular uptake and higher immune activation because of off-target effects. Changes in nanoparticle size and presentation of activating ligands affect construct-induced immune responses at different levels, and care must be taken when considering practical and global design rules for CpG delivery.

TOC graphic

*Corresponding Author: todom@northwestern.edu.

Supporting Information.

Characterizations of CpG and GpC conjugated gold nanoconstructs; Tuning the loading of CpG ODNs on AuNPs through pH-driven method; Cellular uptake of NP-CpG with a constant CpG concentration; Exocytosis profiles of three formulations of NP-CpG constructs; Low overlaying of NP-CpG constructs with lysosomes observed by confocal fluorescence imaging; Time-dependent IS effects of NP-CpG constructs; Higher non-specific IS activity induced by larger constructs; IS activity of three formulations of NP-CpG constructs in the presence of TLR antagonists; Cytokine produced by free form of CpG. This material is available free of charge via the Internet at http://pubs.acs.org.

The authors declare no competing financial interest.

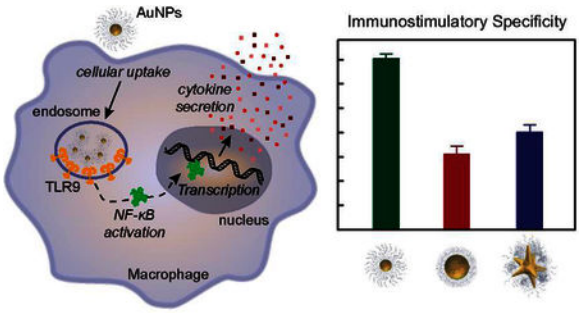

Keywords

Gold nanoparticles; CpG; cellular uptake; immunostimulatory activity; targeting

INTRODUCTION

Toll-like receptors (TLRs) are a class of transmembrane proteins that play a critical role in the immune response to invading pathogens.[1–2] TLR9 is an important endosomal TLR that recognizes DNA sequences that contain unmethylated cytosine-phosphate-guanine (CpG) motifs naturally found in microbes.[3–6] Synthetic oligodeoxynucleotides (ODNs) with CpG moieties designed to artificially stimulate the immune system have, however, poor cellular uptake and are susceptible to degradation by nucleases, which inhibits the targeted downstream immune response of cytokine production.[7–9] In contrast, when densely packed on the surface of nanoparticles (NPs), nucleic acids are more resistant to degradation and display higher cellular uptake,[10–12] which has contributed to the emergence of NP-based constructs to deliver various nucleic acids into cells.[13–14]

Gold nanoparticles (AuNPs) are promising CpG carriers because of their biocompatibility and ease of surface functionalization, but the influence of structural parameters (NP size and shape) on specific immunostimulation responses is unknown because of inconsistent results.[15–21] Reports using AuNPs conjugated with CpG ligands (NP-CpG) indicate opposite conclusions: (1) that larger NP-CpG (80-nm diameter cores) were more immune active than smaller ones in dendritic cells,[15] and (2) that smaller NP-CpG (15-nm diameter cores) were optimal to generate an immune response by activating macrophages.[19–20] The different cell types used in each study suggest that both NP size and cell type affect the immune response. Additionally, the surface density of CpG ODN was inconsistent in those studies. Although reports based on antigen-conjugated AuNPs indicate that different core shapes, including spheres, cubes, and rods, activate different immune responses,[18] there are no reports on whether NP shape influences immunostimulatory effects of NP-CpG.

Because the surface density of CpG on NPs affects TLR9 signaling,[22] lack of comparison using NPs functionalized with CpG ODNs at the same surface density renders any size and shape effects unclear. Also, multi-branched AuNPs such as gold nanostars display different surface curvatures and ligand presentation within the same NP[23–24] and may present distinct immunostimulatory (IS) responses. Free CpG ODNs can bind TLR9 and trigger downstream IS responses; however, the targeting specificity of NP-CpG for TLR9 activation needs

testing to ensure that other pathways are also not stimulated, such as TLRs 7 and 8 that are present in the endosome and activated by viral and bacterial single-stranded RNA oligonucleotides.[25–28] The overstimulation of TLR7/8 is linked to adverse side effects, such as autoimmune disorders,[29] and hence the design of NP-CpG should be taken into consideration when targeting TLR9 for cancer immunotherapy.

Here we show that IS activity depends on NP size at the same CpG density. 13-nm spherical NP-CpG constructs are more specific to TLR9 activation and downstream cytokine production with lower off-target effects. 50-nm spheres and 40-nm stars with similar surface areas showed similar IS behavior, which indicates that shape does not affect specificity of NP-CpG on TLR9 activation. These results indicate that a combination of ligand density and NP structural factors affect different immune responses and that careful attention must be made when designing constructs for eliciting a specific, intended response.

RESULTS AND DISCUSSION

Larger NP-CpG constructs have higher cellular uptake

We synthesized AuNP cores with CpG ligand shells (NP-CpG nanoconstructs) (Scheme 1a-b) by conjugating thiolated CpG ODNs on AuNPs in sodium citrate buffer following our published protocol.[30] To examine effects of NP size, we compared 13-nm and 50-nm spheres and for shape, 40-nm stars and 50-nm spheres (Figure S1) because they have similar surface areas.[31] Since surface density of oligonucleotides on AuNPs affects endocytosis, [30–31] we compared cellular uptake of NP-CpG constructs functionalized with similar CpG surface densities (Table S1). We tuned the CpG loading of each formulation by adjusting the pH of citrate buffer, where the loading of CpG increased with decreased pH (Figure S2).

We selected RAW-Blue macrophages as the model cell line because they express several TLRs, including TLR9, on endosomal membranes[21] that can activate cytokine production after binding with CpG ODNs (Scheme 1c). Because the three nanoconstructs contain a different amount of CpG ODNs on the surface due to the size and surface curvature of the NP core, we adjusted the 13-nm sphere NP-concentration to ~15 and ~17 times higher than 50-nm spheres and 40-nm stars, respectively, to make the overall concentration of CpG prior to cell treatment constant. Cellular uptake of the three NP-CpG constructs was quantified using inductively coupled mass spectrometry (ICP-MS) to determine Au content (number of atoms) per cell. Then, using TEM images of the AuNPs, we estimated the volume of each particle shape (Experimental Section) to determine the number of Au atoms per particle. These two values, Au atoms/cell and Au atoms/AuNP, were used to calculate the number of AuNPs per cell (N_{NPs}/cell) (Figure S3).

Cellular uptake of CpG was estimated by multiplying the N_{NPs}/cell by CpG/AuNP (Figure 1). The uptake of all three formulations increased with time during the initial period (2–16 h) but decreased at later times (24 h). For constructs with different sizes, the maximum uptake of CpG for 50-nm spheres was ~33% higher compared to 13-nm spheres. There was no significant difference on maximum CpG uptake between 50-nm spheres and 40-nm stars.

We hypothesized that two factors may contribute to the decreased cellular uptake at later times: (1) dilution effects caused by cell division,[32] and (2) exocytosis of NP-CpG constructs.[33] RAW-Blue cells typically double between 12–16 h,[34] which reduces the amount of NP-CpG per cell at subsequent time points. To test whether exocytosis contributed to decreased cellular uptake, we quantified exocytosed NP-CpG as a function of time (Experimental Section). Although exocytosis was observed for all three NP-CpG constructs, the overall degree was < 10% over 24 h (Figure S4), which indicates that exocytosis was not a primary factor leading to decreased cellular uptake at later times.

Size influences subcellular locations of NP-CpG constructs

Because TLR9 is located in the endosome, and activation for cytokine production depends on the binding of NP-CpG, endosomal delivery of the constructs is critical. To examine subcellular trafficking of NP-CpG constructs, we immuno-stained endosomes and lysosomes with different fluorophores and monitored locations of the nanoconstructs by confocal laser scanning microscopy (Figure 2). To visualize constructs with fluorescence microscopy, we labeled NP-CpG constructs with Cy5-conjugated dT_{20} oligonucleotides by backfilling (Experimental Section). We analyzed the final surface composition of NP-CpG/Cy5 construct and found that backfilling NP-CpG with dT_{20}-Cy5 did not cause significant changes on the loading of CpG for all three formulations (Table S2).

The subcellular distribution of the three nanoconstructs was qualitatively similar. NP-CpG localized within endosomes or lysosomes at the initial incubation times (2 h), indicated by the high overlap of fluorescence signals from NPs and endosomes (Figure 2) and lysosomes (Figure S5). As the incubation time increased to 16 h, the intensity of the NP-CpG cluster fluorescence inside the organelles decreased for all three formulations. These results suggest that non-co-localized nanoconstructs might be transported to other organelles or reside in the cytoplasm.

Smaller NP-CpG constructs induced higher TLR9 targeting specificity

TLR9 promotes an IS response upon binding with CpG ODNs through activation of the transcription factor (NF-κB) and secretion of biomediators[35] such as enzymes and cytokines (Scheme 1c). Because RAW-Blue cells transfected with NF-κB reporter gene, IS activity can be detected by measuring secreted embryonic alkaline phosphatase (SEAP levels) in cell media (Experimental Section). After treating macrophages with the three NP-CpG formulations (Table S3), we measured SEAP levels to compare whether NP size and shape influenced the IS activity.

The total CpG concentration (C_{CpG}) highly affects the IS activity; therefore, we determined the IS activity of NP-CpG constructs as a function of C_{CpG} (Figure 3a). For all three formulations, IS activity was detected only when $C_{CpG} > 25$ nM. In the range of 25–400 nM, IS activity increased with C_{CpG}. For $C_{CpG} > 400$ nM, the IS activity leveled off, likely because of TLR9 saturation. 50-nm spheres showed slightly higher IS activity compared to 13-nm spheres, and there was no significant difference between 50-nm spheres and 40-nm stars. Furthermore, we investigated the influence of incubation time on IS activity. At the same C_{CpG}, IS activity increased linearly with time (Figure S6). From 2 to 24 h, the IS

activity of 13-nm spheres, 50-nm spheres and 40-nm stars increased by 7.3, 9.2 and 9.0-fold, respectively. In free form, however, CpG showed minimal IS activity over 24 h.

To investigate the TLR9 targeting specificity of NP-CpG constructs on immune activation, we compared against GpC ODNs, a control sequence that contains GpC dinucleotides instead of CpG and does not induce TLR9 activation[36] (NP-GpC, Table S3). We treated RAW-Blue cells with NP-GpC constructs (400 nM in GpC ODN) for 24 h and analyzed the SEAP levels in cell media. Compared to cells treated with PBS (control), 13-nm spherical NP-GpC showed only a slight IS effect, but 50-nm spherical and 40-nm star NP-GpC constructs induced a nearly 4-fold increase of IS activity (Figure S7). To compare quantitatively specificity in TLR9 activation, we normalized IS activity of each of the three formulations by dividing the SEAP level from NP-CpG treated cells by that from NP-GpC treated ones. At the same ODN concentration, 13-nm spheres showed much higher specificity compared to 50-nm spheres, and there was no significant difference between 50-nm spheres and 40-nm stars (Figure 3b). To identify the receptors activated by constructs with the control sequence (NP-GpC), we pre-incubated Raw-Blue macrophages with ODN 2087 and 2088 ligands (500 nM) that block endosomal TLR7/8 and TLR7/8/9 activation, respectively.[37–38] Immune activation of macrophages by larger constructs (GpC functionalized 50-nm spheres and 40-nm stars) decreased when cells were pre-incubated with TLR blockers, which indicates that larger control constructs activated TLR9 and TLR7/8 (Figure 3c). 13-nm spheres with the control sequence, however, did not activate TLR7/8 or 9 since the IS activity did not significantly change after cells were pre-incubated with ODN 2087 or 2088. Therefore, although the GpC sequence in free form does not activate TLRs, when presented on the surface of larger (but not smaller) nanoparticles, NP-GpC can activate TLR7/8 and 9. Finally, we performed similar experiments with NP-CpG and observed that larger particles also induced off-target TLR 7/8 activation when the GpC was replaced by CpG (Figure S8). These results indicate that independently of the DNA sequence, larger NPs functionalized with DNA induced off-target IS response. TRL7, 8, and 9 are colocalized inside the endosomes.[39] Therefore, we hypothesize that larger nanoconstructs (40-nm stars or 50-nm spheres) can interact not only with a single TLR but can also stimulate neighboring receptors to account for the observed off-target effects.

Smaller NP-CpG constructs minimize unintended cytokine production

As downstream products of immunostimulation, cytokines mediate communication between immune cells and boost anticancer immunity.[40–41] To test whether activation of macrophages by NP-CpG constructs induces cytokine secretion, we treated cells with NP-CpG constructs at the same C_{CpG} (400 nM), the concentration that maximized IS activity, for 24 h (Figure 3a). Using a mixture of antibodies that can capture cytokines related to macrophage activation,[42] we analyzed cytokine levels after NP-CpG treatment. Figure 4a shows that all three NP-CpG constructs induced similar levels of cytokine production ($C_{cytokines}$), including pro-inflammatory cytokines (TNF-α, IL-6, G-CSF, LIF),[43] chemokines (RANTES, MIP-2)[44] and immunoregulatory cytokines (IL-10 and IL-13).[45] The composition of cytokines induced by NP-CpG was consistent with the cytokines released by free CpG (Figure S9), and hence conjugation of CpG on AuNPs did not inhibit cytokine production.

To investigate the specificity of NP-CpG on cytokine production, we determined $C_{cytokines}$ in cell media treated by NP-GpC nanoconstructs. At the same C_{GpC} (400 nM), 13-nm spheres induced much lower $C_{cytokines}$ compared to 50-nm spheres, and 40-nm stars showed slightly lower $C_{cytokines}$ compared to 50-nm spheres. We normalized the cytokine concentration ($C_{cytokines,CpG}/C_{cytokines,GpC}$) to compare specificity of the three formulations (Figure 4b). Among the six cytokines that displayed the highest concentrations, we found that 13-nm spheres presented between 2 and 63-fold higher specificity compared to 50-nm spheres. Interestingly, 40-nm stars were more specific in triggering the cytokine production compared to 50-nm spheres. The dependency of specificity of cytokine production on the NP size and shape suggests that the structural parameters of NPs must be considered when using AuNPs as carriers for CpG delivery.

CONCLUSIONS

We identified NP size as a key structural feature on the *in vitro* immunostimulatory response of NP-CpG constructs having the same CpG surface density by comparing 13-nm spheres, 50-nm spheres, and 40-nm stars. Larger constructs (50-nm spheres and 40-nm stars) had higher cellular uptake efficiencies and IS responses from a combination of both target and off-target activation at high concentrations of treatment (400 nM in ODN). Although having lower cellular uptake under the same nanoconstruct concentration, 13-nm spheres had the highest specificity on TLR9-mediated IS responses. These results highlight the complexity of uncovering design principles of nanoconstructs for immune activation because of the interconnected nature of structural parameters and ligand densities and overall concentrations on different IS responses.

EXPERIMENTAL SECTION

Materials

Spherical AuNPs with 13-nm diameter were synthesized by boiling gold(III) chloride trihydrate ($HAuCl_4$, Sigma-Aldrich) in trisodium citrate solution following a published protocol.[46] We synthesized 40-nm gold nanostars following a previously established protocol.[47] CpG ODN (5’-TCC ATG ACG TTC CTG ACG T-3’, phosphodiester (PO) backbone) with a disulfide bond and a spacer phosphoramidite-18 coupled at 3’-end was prepared by solid phase synthesis. Unconjugated spherical AuNPs with 50-nm diameter were purchased from Ted Pella, INC. ODN 2087 and 2088 were purchased from Invivogen. Tris(2-carboxyethyl)phosphine (TCEP) hydrochloride, 11-(mercaptoundecyl)hexa(ethylene glycol) (MUHEG), iodine (I_2), potassium iodide (KI), sodium borohydride ($NaBH_4$), dithiothreitol, hydrochloric acid (HCl, 36–38%), and nitric acid (HNO_3, 70%) were purchased from Sigma-Aldrich. Blocker™ BSA (bovine serum albumin) in phosphate-buffered saline (PBS) (10X), fetal bovine serum (FBS), rabbit serum and Dulbecco’s PBS (DPBS) were purchased from Thermo Fisher Scientific Inc.

Conjugation of CpG or GpC ODNs on Gold Nanoparticles

The conjugation of CpG ODN onto AuNP was performed through pH-driven method. Briefly, the disulfide bond of CpG ODN was first reduced to thiol group in a 20 mM TCEP

solution at room temperature for 30 minutes. TCEP and the cleaved disulfide byproducts were removed by centrifugation with a Amicon Ultra Centrifugal Filter (cutoff size: 3KD). Subsequently, the reduced CpG ODN was mixed with AuNP with a molar ratio (CpG:AuNP) of 200:1 for 13-nm spheres, and 2700:1 for 50-nm spheres and 40-nm stars. The mixture was then shaken at room temperature for 10 min, followed by the addition of trisodium citrate buffer with a final concentration of 10 mM. To tune the loading of CpG, we used the citrate buffer with different pH values (6.5, 4.8 and 3.0). Finally, we backfilled the NP-CpG constructs with 2000-fold excess of MUHEG for 13-nm spheres or 10,000-fold excess of MUHEG for 50-nm spheres and 40-nm stars by shaking the mixture at room temperature for 5 hours. To remove the unconjugated CpG ODN and MUHEG, we performed two centrifugation cycles following our previously published protocol.[31] To quantify the loading of CpG on AuNP, we digested the Au core by sequentially treating the NP-CpG constructs with iodine solution containing 0.16 M I_2 and 1.0 M KI, for 10 min, followed by a reducing solution containing 1: 5 mixture of 2 M $NaBH_4$ and 0.3 M dithiothreitol for 30 min. We centrifuged the solution for 10 min (21,000 × g force), then analyzed the concentration of CpG in the supernatant by the Quant-iT OliGreen ssDNA Assay Kit (Invitrogen™). The number of CpG per AuNP was calculated by dividing the concentration of CpG in the supernatant by that of AuNP core digested in the same supernatant. The concentration of Au nanoconstructs was calculated with the total amount of Au atoms per sample, quantified by ICP-MS (Thermo Fisher Scientific™, iCAP™ Q), and the AuNP average volume, estimated by transmission electron microscopy images.[30] The same protocols were followed for the conjugations and quantifications of GpC ODNs.

Cellular Uptake of Nanoconstructs

Murine RAW-Blue macrophage (InvivoGen™, San Diego, CA), the cell line used in this study for *in vitro* efficiency evaluations, was maintained in growth media composed of Dulbecco's Modified Eagle's medium (Gibco™, ThermoFisher Scientific) supplemented with 4.5 g/L of glucose, 10% of FBS, 200 μg/mL of Zeocin, and 100 ug/mL of Primocin. To evaluate the cellular uptake of CpG constructs, 2×10^5 RAW-Blue cells in 1 mL of growth media were added to each well of a 12-well plate, which was maintained at 37 °C with 5% CO_2 in a humidified incubator. When cells reached ~70% confluence, NP-CpG constructs were added with the concentration of 100 nM (based on CpG). After several time periods (2 h, 8 h, 16 h, and 24 h), the medium was removed and cells on the plate were washed 3 times with DPBS. Cells were then scraped off the plate using a cell scraper (Thermo Scientific™) and transferred to a 1.5 mL of Eppendorf tube and washed for another 2 times with DPBS by centrifugation at the speed of 250 × *g* force for 5 min. Subsequently, we counted the cells in the suspension using a hemocytometer (Marienfeld™). Finally, cells were lysed in the mixture of HCl (2 vol%) and HNO_3(2 vol%) at 70°C overnight for the quantification of gold content by ICP-MS.

Subcellular localization of NP-CpG constructs

To identify the distributions of NP-CpG within cells, we co-conjugated NP-CpG constructs with 5'-Cy5-labeled 20-mers of thymidine (dT_{20}-Cy5) using a 50-fold excess of dT_{20}-Cy5 for 13-nm spheres, or 500-fold excess of dT_{20}-Cy5 for 50-nm spheres and 40-nm stars. One milliliter of RAW-Blue cell suspension in growth medium (2×10^5/mL) were transferred to

a well of a 12-well plate pre-loaded with a round coverslip (d = 12 mm, BD Biosciences), followed by overnight culturing to allow the cells to spread on the coverslip. The cells were then treated with NP-CpG/Cy5 with a similar surface density of oligonucleotides (Table S2). After several time periods (2, 8, or 16 h), cells were washed 3 times with DPBS. To visualize the endosomes and lysosomes, cells were sequentially treated with 4% paraformaldehyde for fixing, 0.1% of Triton X100 for permeabilization, and antibodies for immunostaining, following our previously published protocols.[31]

Immunostimulatory Activity Test by Quanti-Blue Reagent

To test the immunostimulatory activity of NP-CpG constructs, RAW-Blue cells were seeded in a 96-well plate with 1×10^5 cells per well. After adhering to the plate, the cells were treated with NP-CpG constructs at different concentrations (from 0.1 nM to 10 nM for 13-nm spheres and 0.01 nM to 2 nM for 50-nm spheres and 40-nm stars) for several time periods (2, 8, 16, or 24 h). Then the cell culturing medium from each well was collected and centrifuged to remove the constructs that were not taken up by cells. 20 μL of each supernatant was transferred to a well of a new 96-well plate, followed by addition of 200 μL of Quanti-Blue reagent. The plate was maintained at 37 ºC for 6 h, and the absorbance of the solution at 635 nm (OD_{635nm}), which represents the secrete embryonic alkaline phosphatase (SEAP) level released by the NP-CpG constructs, was determined. For the blocking experiments by ODN 2087 and 2088 ligands, RAW-Blue macrophages were pre-incubated with 500 nM of ligands for 2 h before the addition of the nanoconstructs.

Cytokine Detection

RAW-Blue cells were initially seeded in 96-well plates following the same procedure as in the last Section. After 24 h incubation, NP-CpG constructs were added to the cell medium and the concentration of CpG was adjusted to be 400 nM for different formulations. The cells were incubated with NP-CpG constructs for another 24 h, and then the cell culturing medium from each well was centrifuged at 21,000 g × 30 min to remove AuNPs. The supernatant was then collected and analyzed by a Luminex® Multiplex Kit (Mouse ProcartaPlex™, Invitrogen), following the protocols provided by the manufacturer. In brief, 50 μL of magnetic bead solution was added to each well of a 96-well Flat Bottom Plate, and the beads were washed 3-times with the 1X Wash Buffer provided by the kit, using a hand-held magnetic plate washer. Four-time-diluted, NP-CpG-treated cell culturing medium (25 μL) as well as antigen standard (50 μL, provided by the kit) were added to the bead-coated 96-well plate and incubated at room temperature on a shaker at 500 rpm for 1.5 h, followed by 3-times washing. Subsequently, 25 μL of detection antibody mixture was added to each well, and the resulting solutions were incubated at room temperature for 30 min on a plate shaker at 500 rpm. The plate was then washed 3-times to remove unbound antibodies, and 50 μL of streptavidin-PE solution was added to each well. The plate was shaken at 500 rpm for 30 min at room temperature, followed by washing again 3-times. Finally, 120 μL of Reading Buffer (provided by the kit) was added to each well, and after 5 min shaking at room temperature, the solution in each well was analysed by a Luminex® 200 instrument. The concentration of each cytokine was calculated from the calibration curve of the standard antigens.

Supplementary Material

Refer to Web version on PubMed Central for supplementary material.

ACKNOWLEDGMENTS

Research reported in this publication was supported by the National Cancer Institute of the National Institutes of Health under Award Number U54CA199091 (J.Y., R.M.P., C.A.M, A.L., T.W.O.). The content is solely the responsibility of the authors and does not necessarily represent the official views of the National Institutes of Health. L.E.C. acknowledges support from Northwestern University's Cancer Nanotechnology Training Program Award T32CA186897

All the plate-based fluorescence and absorbance readings were carried out in the High Throughput Analysis Laboratory. Confocal fluorescence imaging and TEM were performed at the Biological Imaging Facility. Gold analysis were conducted at the Northwestern University Quantitative Bio-elemental Imaging Center generously supported by NASA Ames Research Center NNA06CB93G.

REFERENCES

1. Takeda K; Akira S Toll-Like Receptors in Innate Immunity. Int. Immunol 2005, 17, 1–14. [PubMed: 15585605]
2. Tosi MF Innate Immune Responses to Infection. J. Allergy Clin. Immunol 2005, 116, 241–249. [PubMed: 16083775]
3. Krieg AM; Vollmer J Toll-Like Receptors 7, 8, and 9: Linking Innate Immunity to Autoimmunity. Immunol. Rev 2007, 220, 251–269. [PubMed: 17979852]
4. Lund J; Sato A; Akira S; Medzhitov R; Iwasaki A Toll-Like Receptor 9-Mediated Recognition of Herpes Simplex Virus-2 by Plasmacytoid Dendritic Cells. J. Exp. Med 2003, 198, 513–520. [PubMed: 12900525]
5. Bauer S; Kirschning CJ; Hacker H; Redecke V; Hausmann S; Akira S; Wagner H; Lipford GB Human Tlr9 Confers Responsiveness to Bacterial DNA Via Species-Specific Cpg Motif Recognition. Proc. Natl. Acad. Sci. U.S.A 2001, 98, 9237–9242. [PubMed: 11470918]
6. Hemmi H; Takeuchi O; Kawai T; Kaisho T; Sato S; Sanjo H; Matsumoto M; Hoshino K; Wagner H; Takeda K; Akira S A Toll-Like Receptor Recognizes Bacterial DNA. Nature 2000, 408, 740–745. [PubMed: 11130078]
7. Krieg AM Therapeutic Potential of Toll-Like Receptor 9 Activation. Nat. Rev. Drug Discov 2006, 5, 471–484. [PubMed: 16763660]
8. Bode C; Zhao G; Steinhagen F; Kinjo T; Klinman DM Cpg DNA as a Vaccine Adjuvant. Expert Rev. Vaccines 2011, 10, 499–511. [PubMed: 21506647]
9. Levin AA A Review of the Issues in the Pharmacokinetics and Toxicology of Phosphorothioate Antisense Oligonucleotides. Biochim. Biophys. Acta 1999, 1489, 69–84. [PubMed: 10806998]
10. Seferos DS; Prigodich AE; Giljohann DA; Patel PC; Mirkin CA Polyvalent DNA Nanoparticle Conjugates Stabilize Nucleic Acids. Nano Lett 2009, 9, 308–311. [PubMed: 19099465]
11. Rosi NL; Giljohann DA; Thaxton CS; Lytton-Jean AK; Han MS; Mirkin CA Oligonucleotide-Modified Gold Nanoparticles for Intracellular Gene Regulation. Science 2006, 312, 1027–1030. [PubMed: 16709779]
12. Choi CH; Hao L; Narayan SP; Auyeung E; Mirkin CA Mechanism for the Endocytosis of Spherical Nucleic Acid Nanoparticle Conjugates. Proc. Natl. Acad. Sci. U.S.A 2013, 110, 7625–7630. [PubMed: 23613589]
13. Ding Y; Jiang Z; Saha K; Kim CS; Kim ST; Landis RF; Rotello VM Gold Nanoparticles for Nucleic Acid Delivery. Mol. Ther 2014, 22, 1075–1083. [PubMed: 24599278]
14. Li W; Szoka FCJ Lipid-Based Nanoparticles for Nucleic Acid Delivery. Pharm. Res 2007, 24, 438–449. [PubMed: 17252188]
15. Zhou Q; Zhang Y; Du J; Li Y; Zhou Y; Fu Q; Zhang J; Wang X; Zhan L Different-Sized Gold Nanoparticle Activator/Antigen Increases Dendritic Cells Accumulation in Liver-Draining Lymph Nodes and Cd8+ T Cell Responses. ACS Nano 2016, 10, 2678–2692. [PubMed: 26771692]

16. Tao Y; Ju EG; Li ZH; Ren JS; Qu XG Engineered Cpg-Antigen Conjugates Protected Gold Nanoclusters as Smart Self-Vaccines for Enhanced Immune Response and Cell Imaging. Adv. Funct. Mater. 2014, 24, 1004–1010.
17. Chen N; Wei M; Sun Y; Li F; Pei H; Li X; Su S; He Y; Wang L; Shi J; Fan C; Huang Q Self-Assembly of Poly-Adenine-Tailed Cpg Oligonucleotide-Gold Nanoparticle Nanoconjugates with Immunostimulatory Activity. Small 2014, 10, 368–375. [PubMed: 23963797]
18. Niikura K; Matsunaga T; Suzuki T; Kobayashi S; Yamaguchi H; Orba Y; Kawaguchi A; Hasegawa H; Kajino K; Ninomiya T; Ijiro K; Sawa H Gold Nanoparticles as a Vaccine Platform: Influence of Size and Shape on Immunological Responses in Vitro and in Vivo. Acs Nano 2013, 7, 3926–3938. [PubMed: 23631767]
19. Lin AY; Almeida JP; Bear A; Liu N; Luo L; Foster AE; Drezek RA Gold Nanoparticle Delivery of Modified Cpg Stimulates Macrophages and Inhibits Tumor Growth for Enhanced Immunotherapy. PLoS One 2013, 8, e63550. [PubMed: 23691064]
20. Wei M; Chen N; Li J; Yin M; Liang L; He Y; Song H; Fan C; Huang Q Polyvalent Immunostimulatory Nanoagents with Self-Assembled Cpg Oligonucleotide-Conjugated Gold Nanoparticles. Angew. Chem. Int. Ed. Engl. 2012, 51, 1202–1206. [PubMed: 22190176]
21. Radovic-Moreno AF; Chernyak N; Mader CC; Nallagatla S; Kang RS; Hao L; Walker DA; Halo TL; Merkel TJ; Rische CH; Anantatmula S; Burkhart M; Mirkin CA; Gryaznov SM Immunomodulatory Spherical Nucleic Acids. Proc. Natl. Acad. Sci. U.S.A. 2015, 112, 3892–3897. [PubMed: 25775582]
22. Leleux JA; Pradhan P; Roy K Biophysical Attributes of Cpg Presentation Control Tlr9 Signaling to Differentially Polarize Systemic Immune Responses. Cell Rep. 2017, 18, 700–710. [PubMed: 28099848]
23. Lee H; Dam DH; Ha JW; Yue J; Odom TW Enhanced Human Epidermal Growth Factor Receptor 2 Degradation in Breast Cancer Cells by Lysosome-Targeting Gold Nanoconstructs. ACS Nano 2015, 9, 9859–9867. [PubMed: 26335372]
24. Dam DHM; Lee JH; Sisco PN; Co DT; Zhang M; Wasielewski MR; Odom TW Direct Observation of Nanopariticle-Cancer Cell Nucleus Interactions. ACS Nano 2012, 6, 3318–3326. [PubMed: 22424173]
25. Cervantes JL; Weinerman B; Basole C; Salazar JC Tlr8: The Forgotten Relative Revindicated. Cell. Mol. Immunol 2012, 9, 434–438. [PubMed: 23085951]
26. Kawai T; Akira S Toll-Like Receptor Downstream Signaling. Arthritis Res. Ther. 2005, 7, 12–19.
27. Heil F; Hemmi H; Hochrein H; Ampenberger F; Kirschning C; Akira S; Lipford G; Wagner H; Bauer S Species-Specific Recognition of Single-Stranded Rna Via Toll-Like Receptor 7 and 8. Science 2004, 303, 1526–1529. [PubMed: 14976262]
28. Diebold SS; Kaisho T; Hemmi H; Akira S; Reis e Sousa C Innate Antiviral Responses by Means of Tlr7-Mediated Recognition of Single-Stranded Rna. Science 2004, 303, 1529–1531. [PubMed: 14976261]
29. Nickerson KM; Christensen SR; Shupe J; Kashgarian M; Kim D; Elkon K; Shlomchik MJ Tlr9 Regulates Tlr7- and Myd88-Dependent Autoantibody Production and Disease in a Murine Model of Lupus. J. Immunol. 2010, 184, 1840–1848. [PubMed: 20089701]
30. Dam DH; Lee RC; Odom TW Improved in Vitro Efficacy of Gold Nanoconstructs by Increased Loading of G-Quadruplex Aptamer. Nano Lett. 2014, 14, 2843–2848. [PubMed: 24689438]
31. Yue J; Feliciano TJ; Li W; Lee A; Odom TW Gold Nanoparticle Size and Shape Effects on Cellular Uptake and Intracellular Distribution of Sirna Nanoconstructs. Bioconjug. Chem 2017, 28, 1791–1800. [PubMed: 28574255]
32. Kim JA; Aberg C; Salvati A; Dawson KA Role of Cell Cycle on the Cellular Uptake and Dilution of Nanoparticles in a Cell Population. Nat. Nanotechnol 2011, 7, 62–68. [PubMed: 22056728]
33. Oh N; Park JH Endocytosis and Exocytosis of Nanoparticles in Mammalian Cells. *Int. J. Nanomedicine* 2014, 9Suppl 1, 51–63.
34. Bancos S; Tyner KM Evaluating the Effect of Assay Preparation on the Uptake of Gold Nanoparticles by Raw264.7 Cells. *J. Nanobiotechnology* 2014, 12, 45. [PubMed: 25424488]

35. Takeshita F; Gursel I; Ishii KJ; Suzuki K; Gursel M; Klinman DM Signal Transduction Pathways Mediated by the Interaction of Cpg DNA with Toll-Like Receptor 9. Semin. Immunol. 2004, 16, 17–22. [PubMed: 14751759]

36. Decker T; Schneller F; Sparwasser T; Tretter T; Lipford GB; Wagner H; Peschel C Immunostimulatory Cpg-Oligonucleotides Cause Proliferation, Cytokine Production, and an Immunogenic Phenotype in Chronic Lymphocytic Leukemia B Cells. Blood 2000, 95, 999–1006. [PubMed: 10648415]

37. Krieg AM; Wu T; Weeratna R; Efler SM; Love-Homan L; Yang L; Yi AK; Short D; Davis HL Sequence Motifs in Adenoviral DNA Block Immune Activation by Stimulatory Cpg Motifs. Proc. Natl. Acad. Sci. U.S.A. 1998, 95, 12631–12636. [PubMed: 9770537]

38. Stunz LL; Lenert P; Peckham D; Yi AK; Haxhinasto S; Chang M; Krieg AM; Ashman RF Inhibitory Oligonucleotides Specifically Block Effects of Stimulatory Cpg Oligonucleotides in B Cells. Eur. J. Immunol. 2002, 32, 1212–1222. [PubMed: 11981808]

39. Wang JY; Shao Y; Bennett TA; Shankar RA; Wightman PD; Reddy LG The Functional Effects of Physical Interactions among Toll-Like Receptors 7, 8, and 9. J. Biol. Chem. 2006, 281, 37427–37434. [PubMed: 17040905]

40. Stenger S; Rollinghoff M Role of Cytokines in the Innate Immune Response to Intracellular Pathogens. Ann. Rheum. Dis. 2001, 60 Suppl 3, iii43–iii46.

41. Arango Duque G; Descoteaux A Macrophage Cytokines: Involvement in Immunity and Infectious Diseases. Front. Immunol 2014, 5, 491. [PubMed: 25339958]

42. Baker HN; Murphy R; Lopez E; Garcia C Conversion of a Capture Elisa to a Luminex Xmap Assay Using a Multiplex Antibody Screening Method. J. Vis. Exp. 2012, e4084.

43. Dinarello CA Proinflammatory Cytokines. Chest 2000, 118, 503–508. [PubMed: 10936147]

44. Graves DT; Jiang Y Chemokines, a Family of Chemotactic Cytokines. Crit. Rev. Oral Biol. Med. 1995, 6, 109–118. [PubMed: 7548618]

45. Sultani M; Stringer AM; Bowen JM; Gibson RJ Anti-Inflammatory Cytokines: Important Immunoregulatory Factors Contributing to Chemotherapy-Induced Gastrointestinal Mucositis. Chemother. Res. Pract 2012, 2012, 490804. [PubMed: 22973511]

46. Li C; Li D; Wan G; Xu J; Hou W Facile Synthesis of Concentrated Gold Nanoparticles with Low Size-Distribution in Water: Temperature and Ph Controls. Nanoscale Res. Lett 2011, 6, 440. [PubMed: 21733153]

47. Chandra K; Culver KSB; Werner SE; Lee RC; Odom TW Manipulating the Anisotropic Structure of Gold Nanostars Using Good's Buffers. Chem. Mater 2016, 28, 6763–6769.

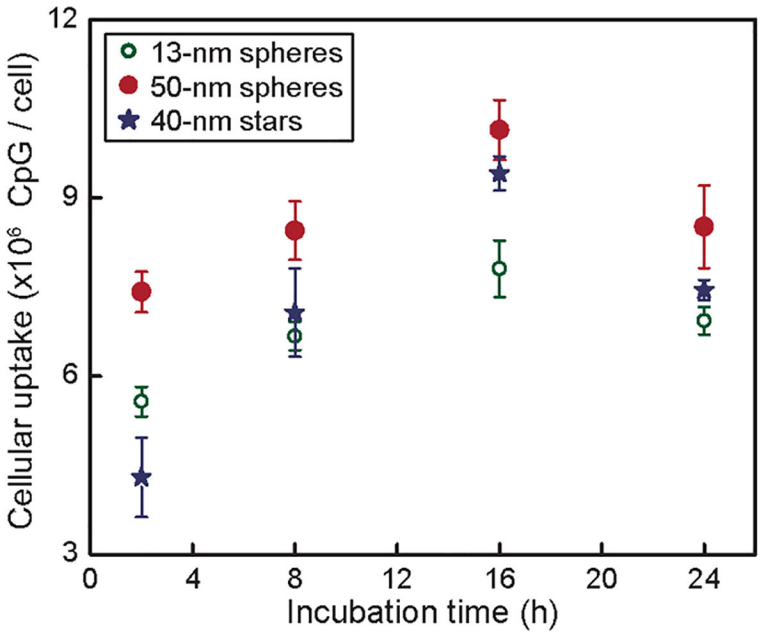

Figure 1. Larger NP-CpG nanoconstructs showed higher efficiency of cellular uptake of CpG compared to smaller ones.

Cellular uptake of three NP-CpG constructs was tested at the same concentration of CpG (100 nM).

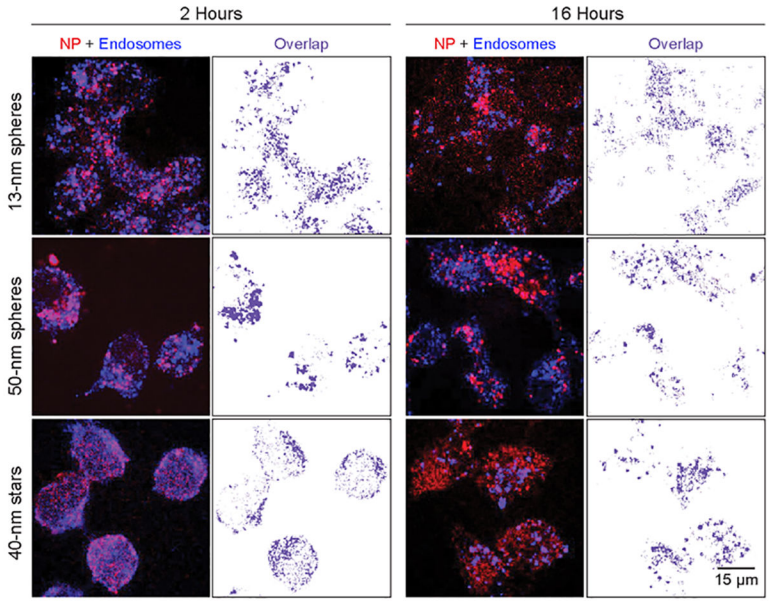

Figure 2. Confocal fluorescent images indicate that the three NP-CpG constructs display similar subcellular locations.

To track NPs inside cells, NP-CpG constructs were backfilled with a Cy5-labeled poly(T) (red). Endosomes were immuno-stained with EEA-1 antibody (blue). Purple color indicates the extracted overlaying signals of constructs and endosomes. Scale bars are 15 μm for all images, and the area visualized 68 × 68 um^2.

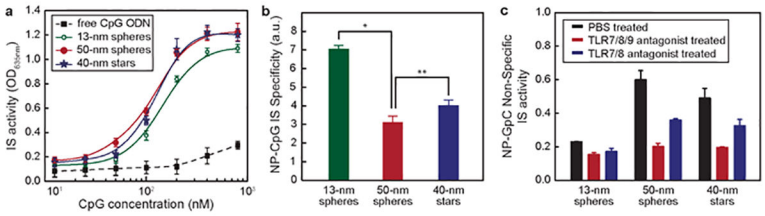

Figure 3. Smaller constructs induced higher IS specificity.

(a) RAW-Blue macrophages were treated with three NP-CpG for 24 h, and the SEAP levels in media were analyzed to give the IS activity; (b) IS specificity was calculated by dividing the IS activity from NP-CpG constructs by that from NP-GpC at the same concentration of ODNs (400 nM). *$p < 0.01$; **$p > 0.05$. (c) IS activity of three formulations of NP-GpC constructs in the presence of TLR antagonists (500 nM).

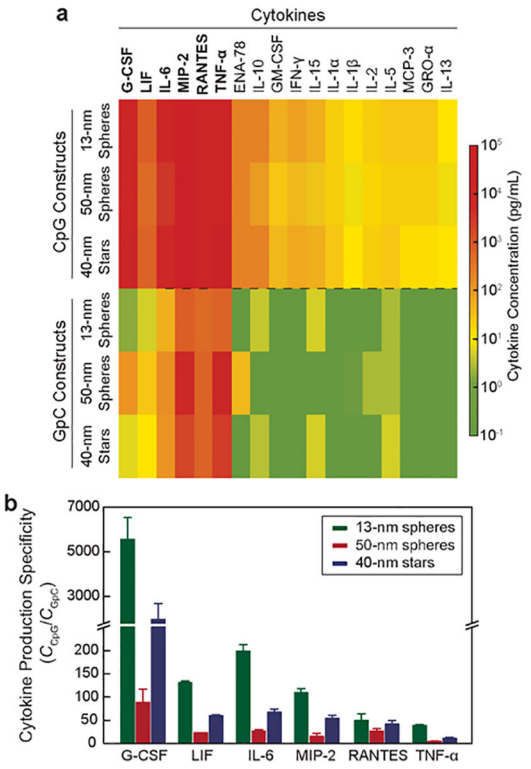

Figure 4. 13-nm spheres showed the highest specificity in the production of cytokines.

(a) Concentration heat-map of cytokines produced by NP-CpG and NP-GpC constructs. **(b)** Specificity of cytokine production was calculated by dividing the concentration of cytokines from NP-CpG by that from NP-GpC.

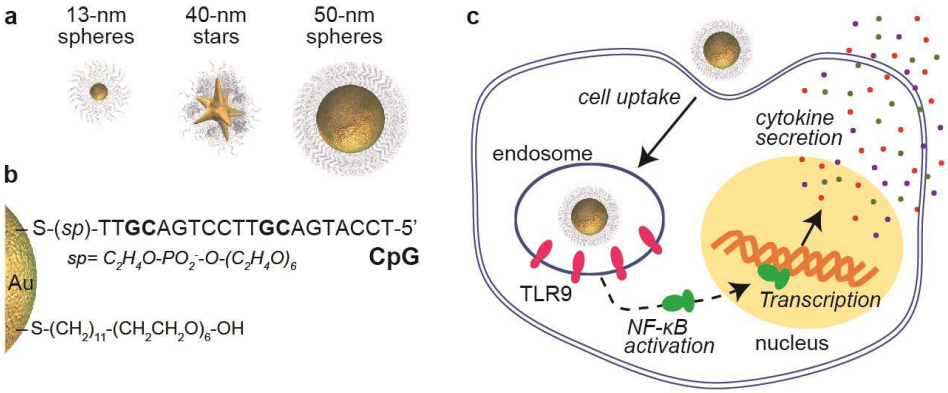

Scheme 1. Side-by-side comparison of size and shape effects on the *in vitro* efficacy of NP-CpG constructs.

. Core structures (a) and surface composition (b) of NP-CpG constructs; (c) the Cellular uptake, immunostimulatory activity, and production of cytokines of NP-CpG constructs with TLR9-expressing macrophages were investigated